Metal Complexes in Inorganic Matrices. 11.[1] Composition of Highly Dispersed Bimetallic Ni, Pd Alloy Particles Prepared by Sol–Gel Processing: Electron Microscopy and Ferromagnetic Resonance Study

Wolfgang Mörke,[†] Ryszard Lamber,[‡] Ulrich Schubert,[*,§,⊥] and Boris Breitscheidel[§]

Institut für Analytik und Umweltchemie, Universität Halle-Wittenberg, Geusaer Strasse, D-06217 Merseburg, Germany; Institut für Angewandte und Physikalische Chemie, Universität Bremen, Bibliotheksstrasse, D-28359 Bremen, Germany; and Institut für Anorganische Chemie, Universität Würzburg, Am Hubland, D-97074 Würzburg, Germany

Received February 28, 1994. Revised Manuscript Received July 18, 1994[⊗]

The composites Pd_xNi_{1-x}·$15SiO_2$ (x = 0.1, 0.3, 0.5, 0.7, or 0.9) with highly dispersed Ni/Pd alloy particles in a silica matrix were prepared by sol–gel processing, starting from Pd(acac)$_2$, Ni(OAc)$_2$, Si(OEt)$_4$, and $H_2NCH_2CH_2NH(CH_2)_3Si(OEt)_3$. The gels were calcined at 823 K in air and finally reduced with H_2 at 773 K. Transmission electron micrographs of Pd_xNi_{1-x}·$15SiO_2$ revealed a bimodal particle size distribution, with 4–6 nm diameters for the smaller and 14–20 nm for the larger particles. The fcc lattice constants, determined by electron diffraction, showed the smaller particles to have about the nominal composition while the larger particles are richer in Pd. The particle compositions were independently determined from the Curie temperatures, obtained by thermomagnetic measurements, and the particle diameters from the I_{rel}^{exp} values. By simulation of the FMR (ferromagnetic resonance) powder spectra, a third, Pd-rich, composition was identified (for Pd_xNi_{1-x} with $x \geq 0.3$). Since the Ni-rich particles have approximately the nominal composition and the other particles are richer in Pd, there has to be additional, probably unreduced nickel in the bulk of the material. To reach a good fit between experimental and calculated spectra, one has to calculate the spectra with a B value smaller than B_0. This is interpreted by tension on the metal particles and may be caused by the presence of unreduced Ni^{2+}, which probably anchors the alloy particles to the matrix. This conclusion is supported by the magnitude of the anisotropy field in the Ni-rich crystallites.

Introduction

Highly dispersed metals deposited on high-surface-area, porous oxidic supports play a very important role in both laboratory and industrial catalysis. They are mostly prepared by H_2 reduction or thermal decomposition of the metal oxides or salts previously deposited on the support by either impregnation or ion exchange. Carrier and the precursor of the metal may also be prepared in one chemical operation, i.e., by coprecipitation or sol–gel processing.

Impregnation is a very simple method. However, the metal particle size and the particle distribution are difficult to control. The same is true for coprecipitation. Contrary to that, the sol–gel process allows both the generation of very small metal particles (<2–5 nm) with narrow distributions and the tailoring of the support properties. The key to control the metal particle size is the high dispersion of the metal precursor during the sol–gel step. Anchoring of the metal precursor to the support via E–O–M links (E = Si, Al, etc.; M = transition metal) gave very good results in several cases.[2] However, not every metal forms stable E–O–M bonds.

We therefore developed a more general method. Instead of linking the metal ions to the silicate network during sol–gel processing by oxo bridges, organic groupings were used. These are provided by the readily available compounds $(RO)_3Si–X–A$. The group A is an organic function capable of coordinating to metal ions, and X is a chemically inert spacer, for instance, a $(CH_2)_n$ chain. While there is no possibility of modifying the M–O–Si links, the M–A–X–Si grouping is easily adjusted to the requirements of a particular metal or to particular reaction conditions. The new method allowed the preparation of composites even with a high metal loading (up to a composition of M·SiO_2). The particles were statistically dispersed in the matrix and had narrow and Gaussian-shaped size distributions.[3]

The dispersed metals were prepared by a three-step procedure. In the first step an alcoholic solution of a metal salt, an (aminoalkyl)silane $R'HN(CH_2)_3Si(OR)_3$ (R' = H or $H_2N(CH_2)_2$) and $Si(OR)_4$ was processed by the sol–gel method. From the M:Si ratio of the starting

[†] Universität Halle-Wittenberg.
[‡] Universität Bremen.
[§] Universität Würzburg.
[⊥] New address: Institut für Anorganische Chemie der Technischen Universität Wien, Getreidemarkt 9, A-1060 Wien, Austria.
[⊗] Abstract published in *Advance ACS Abstracts,* September 1, 1994.
(1) Part 10: Buhler, H.; Schubert, U. *Chem. Ber.* **1993**, *126*, 405.

(2) Leading references: Ueno, A.; Suzuki, H.; Kotera, Y. *J. Chem. Soc., Faraday Trans. 1* **1983**, *79*, 127. López, T.; Bosch, P.; Morán, M.; Gómez, R. *J. Phys. Chem.* **1993**, *97*, 1671.

(3) (a) Breitscheidel, B.; Zieder, J.; Schubert, U. *Chem. Mater.* **1991**, *3*, 559. (b) Schubert, U.; Breitscheidel, B.; Buhler, H.; Egger, C.; Urbaniak, W. *Mater. Res. Soc. Symp. Proc.* **1992**, *271*, 621. (c) Petrullat, J.; Ray, S.; Schubert, U.; Guldner, G.; Egger, C.; Breitscheidel, B. *J. Non-Cryst. Solids* **1992**, *147, 148*, 594.

0897-4756/94/2806-1659$04.50/0

Scheme 1

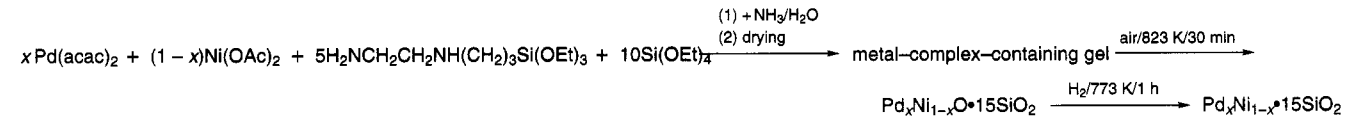

compounds the later composition of the composite is determined. The amino groups of the starting silane coordinate to the metal ions, and the resulting metal complexes are anchored to the silicate matrix during sol–gel processing. Aggregation of the metal ions during sol–gel processing is thus prevented. In the second step the metal-complex-containing gels are heat-treated in air to oxidize all organic moieties. Due to the high dispersion of the metal ions in the first step, small metal oxide particles are formed, which are then reduced to metal particles having diameters of a few nanometers.

The final metal particle size mainly depends on the kind of metal and the oxidation conditions but also on the nature of the organic anchoring group.[3b] This observation indicates that the mechanism of particle growth is rather complicated.

Alloying of a dispersed metal catalyst with a second metal is often desirable to achieve a better activity or selectivity. Due to the advantages of the sol–gel process for preparing highly dispersed monometallic particles, preparation of bimetallic particles by this route could also be advantageous.

We applied the $(RO)_3Si-X-A$ method to mixtures of two different metal ions and chose the Ni/Pd system for three reasons: (i) the monometallic systems Ni/SiO_2 and Pd/SiO_2 were very well studied in our previous investigations,[3] (ii) the metals form solid solutions for any Ni/Pd ratio when they are alloyed at high temperatures, and (iii) the presence of Ni allows the application of magnetic methods to determine the metal particle composition and size.

$Ni{\cdot}13SiO_2$ was previously prepared from $Ni(OAc)_2$, 3 equiv of $H_2NCH_2CH_2NH(CH_2)_3Si(OEt)_3$, and 10 equiv of $Si(OEt)_4$ (oxidation at 823 K/30 min, reduction at 1173 K/2 h) and had a mean Ni particle diameter of 22.9 nm. $Pd{\cdot}15SiO_2$, prepared from $Pd(acac)_2$, 5 equiv of $H_2NCH_2CH_2NH(CH_2)_3Si(OEt)_3$, and 10 equiv of $Si(OEt)_4$ (oxidation at 823 K/30 min, reduction at 773 K/1 h), had a mean Pd particle diameter of 3.8 nm. While the mean Pd particle size was rather independent of the metal loading and the reduction temperature, the mean Ni size diameter was influenced by both parameters. The mean diameter increased from 5.9 nm in $Ni{\cdot}33SiO_2$ to 50.3 nm in $Ni{\cdot}SiO_2$. There was a monodispersed particle size distribution at low and high metal loadings. A bimodal particle size distribution was found in the intermediate range ($Ni{\cdot}ySiO_2$, $y = 2-5.5$), the smaller particles being centered around 5–10 nm and the larger ones around 40–90 nm. A higher reduction temperature causes an increase of the mean particle size and a broadening of the particle size distribution curve.

In this paper we report the properties of a series of bimetallic composites $Pd_xNi_{1-x}{\cdot}15SiO_2$ (**1**–**5**; nominal compositions: **1**, $Pd_{0.9}Ni_{0.1}{\cdot}15SiO_2$; **2**, $Pd_{0.7}Ni_{0.3}{\cdot}15SiO_2$; **3**, $Pd_{0.5}Ni_{0.5}{\cdot}15SiO_2$; **4**, $Pd_{0.3}Ni_{0.7}{\cdot}15SiO_2$; **5**, $Pd_{0.1}Ni_{0.9}{\cdot}15SiO_2$) with x ranging from 0.1 to 0.9. We deliberately used the same reaction conditions as for the preparation of the monometallic systems to make all systems comparable.

Two limiting cases are possible: separation of the two metals might occur during the preparation, in either the oxidation or the reduction step. The other extreme would be the formation of monodisperse bimetallic particles, all having the same composition. The question on how the particles are composed is addressed in this paper.

Experimental Section

Preparation of the Materials. The bimetallic composites **1**–**5** were prepared in a three-step procedure (Scheme 1), as described for the monometallic composites $M{\cdot}xSiO_2$.[3] Step 1: 5.60 g (20.0 mmol) of $H_2NCH_2CH_2NH(CH_2)_3(OEt)_3$ was added to a suspension of $Pd(acac)_2$ and $Ni(OAc)_2$ (together 4.0 mmol) in 400 mL of ethanol. The mixture was stirred at room temperature until a clear solution was obtained (about 1 h). $Si(OEt)_4$ (8.32 mL, 40.0 mmol) was then added, followed by aqueous ammonia (29.70 mL, 1.65 mol, 0.2 N). The mixture was heated to 343 K for 72 h, and then the solvent was removed at 333 K/12 Torr. The obtained nonporous xerogels were dried at 343 K/10^{-3} Torr and analyzed by elemental analysis.

Step 2: For removal of the organic moieties the xerogels were calcined in air at 823 K for 30 min as described in ref 2. Elemental analyses showed that the carbon was nearly completely removed; the analytical composition of the composites at this stage corresponded to $Pd_xNi_{1-x}O{\cdot}15SiO_2$.

Step 3: Reduction with H_2 at 773 K for 1 h gave the composites **1**–**5**.

1: 1.096 g (3.6 mmol) of $Pd(acac)_2$ and 0.100 g (0.4 mmol) of $Ni(OAc)_2$.

Step 1: Anal. Calcd for $[C_{10}H_{14}O_4Pd]_{0.9}{\cdot}[C_4H_6O_4Ni]_{0.1}{\cdot}C_{25}H_{65}N_{10}O_{27.5}Si_{15}$: C, 24.92; H, 4.72; N, 8.45; Pd, 5.78; Ni, 0.35. Found: C, 24.91; H, 5.27; N, 7.67; Pd, 5.68; Ni, 0.36.

Step 2: Specific surface area 450 m^2/g; specific pore volume 0.054 cm^3/g; mean pore radius 1.3 nm. Anal. Calcd for $Si_{15}Ni_{0.1}O_{31}Pd_{0.9}$: C, 0.0; H, 0.0; N, 0.0; Pd, 9.41; Ni, 0.58. Found: C, 0.0; H, 0.47; N, 0.0; Pd, 8.81; Ni, 0.55.

Step 3: Specific surface area 448 m^2/g; specific pore volume 0.082 cm^3/g; mean pore radius 2.0 nm. Anal. Calcd for $Si_{15}Ni_{0.1}O_{30}Pd_{0.9}$: C, 0.0; H, 0.0; N, 0.0; Pd, 9.56; Ni, 0.59. Found: C, 0.0; H, 0.34; N, 0.0; Pd, 8.89; Ni, 0.54.

2: 0.852 g (2.8 mmol) of $Pd(acac)_2$ and 0.299 g (1.2 mmol) of $Ni(OAc)_2$.

Step 1: Anal. Calcd for $[C_{10}H_{14}O_4Pd]_{0.7}{\cdot}[C_4H_6O_4Ni]_{0.3}{\cdot}C_{25}H_{65}N_{10}O_{27.5}Si_{15}$: C, 24.42; H, 4.70; N, 8.58; Pd, 4.57; Ni, 1.08. Found: C, 24.25; H, 5.35; N, 8.15; Pd, 4.35; Ni, 1.06.

Step 2: Specific surface area 480 m^2/g; specific pore volume 0.050 cm^3/g; mean pore radius 1.3 nm. Anal. Calcd for $Si_{15}Ni_{0.3}O_{31}Pd_{0.7}$: C, 0.0; H, 0.0; N, 0.0; Pd, 7.39; Ni, 1.78. Found: C, 0.24; H, 0.42; N, 0.0; Pd, 6.96; Ni, 1.58.

Step 3: Specific surface area 472 m^2/g; specific pore volume 0.049 cm^3/g; mean pore radius 1.3 nm. Anal. Calcd for $Si_{15}Ni_{0.3}O_{30}Pd_{0.7}$: C, 0.0; H, 0.0; N, 0.0; Pd, 7.51; Ni, 1.78. Found: C, 0.0; H, 0.58; N, 0.0; Pd, 6.80; Ni, 1.58.

3: 0.609 g (2.0 mmol) of $Pd(acac)_2$ and 0.498 g (2.0 mmol) of $Ni(OAc)_2$.

Step 1: Anal. Calcd for $[C_{10}H_{14}O_4Pd]_{0.5}{\cdot}[C_4H_6O_4Ni]_{0.5}{\cdot}C_{25}H_{65}N_{10}O_{27.5}Si_{15}$: C, 23.91; H, 4.67; N, 8.72; Pd, 3.31; Ni, 1.83. Found: C, 23.54; H, 5.03; N, 8.16; Pd, 3.15; Ni, 1.71.

Step 2: Specific surface area 492 m^2/g; specific pore volume 0.152 cm^3/g; mean pore radius 1.2 nm. Anal. Calcd for $Si_{15}Ni_{0.5}O_{31}Pd_{0.5}$: C, 0.0; H, 0.0; N, 0.0; Pd, 5.33; Ni, 2.94. Found: C, 0.0; H, 0.43; N, 0.0; Pd, 4.74; Ni, 2.74.

Step 3: Specific surface area 499 m^2/g; specific pore volume 0.189 cm^3/g; mean pore radius 1.6 nm. Anal. Calcd for

$Si_{15}Ni_{0.5}O_{30}Pd_{0.5}$: C, 0.0; H, 0.0; N, 0.0; Pd, 5.41; Ni, 2.99. Found: C, 0.0; H, 0.27; N, 0.0; Pd, 4.74; Ni, 2.75.

4: 0.365 (1.2 mmol) $Pd(acac)_2$ and 0.697 g (2.8 mmol) $Ni(OAc)_2$.

Step 1: Anal. Calcd for $[C_{10}H_{14}O_4Pd]_{0.3}[C_4H_6O_4Ni]_{0.7}C_{25}H_{65}N_{10}O_{27.5}Si_{15}$: C, 23.39; H, 4.65; N, 8.86; Pd, 2.02; Ni, 2.60. Found: C, 23.19; H, 5.15; N, 8.37; Pd, 1.88; Ni, 2.42.

Step 2: Specific surface area 504 m^2/g; specific pore volume 0.090 cm^3/g; mean pore radius 1.5 nm. Anal. Calcd for $Si_{15}Ni_{0.7}O_{31}Pd_{0.}$: C, 0.0; H, 0.0; N, 0.0; Pd, 3.23; Ni, 4.15. Found: C, 0.0; H, 0.43; N, 0.0; Pd, 2.85; Ni, 3.74.

Step 3: Specific surface area 495 m^2/g; specific pore volume 0.092 cm^3/g; mean pore radius 1.6 nm. Anal. Calcd for $Si_{15}Ni_{0.7}O_{30}Pd_{0.3}$: C, 0.0; H, 0.0; N, 0.0; Pd, 3.28; Ni, 4.22. Found: C, 0.0; H, 0.23; N, 0.0; Pd, 2.76; Ni, 3.46.

5: 0.122 g (0.4 mmol) of $Pd(acac)_2$ and 0.896 g (3.6 mmol) of $Ni(OAc)_2$.

Step 1: Anal. Calcd for $[C_{10}H_{14}O_4Pd]_{0.1}[C_4H_6O_4Ni]_{0.9}C_{25}H_{65}N_{10}O_{27.5}Si_{15}$: C, 22.85; H, 4.62; N, 9.01; Pd, 0.68; Ni, 3.40. Found: C, 22.36; H, 4.50; N, 7.33; Pd, 0.65; Ni, 3.20.

Step 2: Specific surface area 492 m^2/g; specific pore volume 0.098 cm^3/g; mean pore radius 1.7 nm. Anal. Calcd for $Si_{15}Ni_{0.9}O_{31}Pd_{0.1}$: C, 0.0; H, 0.0; N, 0.0; Pd, 1.09; Ni, 5.39. Found: C, 0.70; H, 0.48; N, 0.0; Pd, 0.88; Ni, 5.02.

Step 3: Specific surface area 493 m^2/g; specific pore volume 0.134 cm^3/g; mean pore radius 2.2 nm. Anal. Calcd for $Si_{15}Ni_{0.9}O_{31}Pd_{0.1}$: C, 0.0; H, 0.0; N, 0.0; Pd, 1.10; Ni, 5.48. Found: C, 0.20; H, 0.57; N, 0.0; Pd, 1.03; Ni, 5.06.

FMR investigations were performed in the temperature range between 123 K and the Curie temperature at about 600 K, using an X-band spectrometer (ERS 220, ZWG Berlin). The samples were reduced at 578 K in a stream of H_2 (3 L/h), cooled to room temperature in an Ar atmosphere, and sealed in glass tubes prior to the FMR measurements. The experimental FMR intensity (I_{rel}^{exp}) was calculated according to ref 4. The composition of the particles was deduced from the Curie temperature (T_c). T_c was determined by extrapolation of the linear parts of the I_{rel}^{exp} curve to the T axis[5] with an estimated error of ±10 K. From that, the error in the atomic composition of the particles is ±3%.

Temperature-programed reduction (TPR) was performed according to ref 6 on samples that were reoxidized in air at room temperature.

Transmission electron microscopy (TEM) was carried out with a Philips EM 420 T electron microscope operated at 120 kV and equipped with an energy-dispersive X-ray analyzer (EDX). The samples were ground to a fine powder, deposited on copper grids coated with a carbon film and dispersed on the grid ultrasonically. No organic solvents were used during this procedure. Details on the technique are reported in ref 7.

Results

Transmission Electron Microscopy. A transmission electron micrograph (TEM) of **2** (Pd:Ni = 7:3) is shown in Figure 1. There are metal particles with diameters in the range 4–6 nm. A minor fraction consists of large particles with diameters of 14–20 nm. Electron diffraction analyses (ED) revealed fcc diffraction rings corresponding to average lattice constants $a_1 = 0.379 \pm 0.003$ nm and $a_2 = 0.388 \pm 0.003$ nm (Table 1). Figure 2a shows the EDX spectrum from sample areas free from large metal particles, and Figure 2b the EDX spectrum when the electron probe was focused on a large metal particle. Analysis of Figure 2 reveals some differences in the composition of small and large metal particles. The larger particles contain a higher concentration of Pd than the smaller ones.

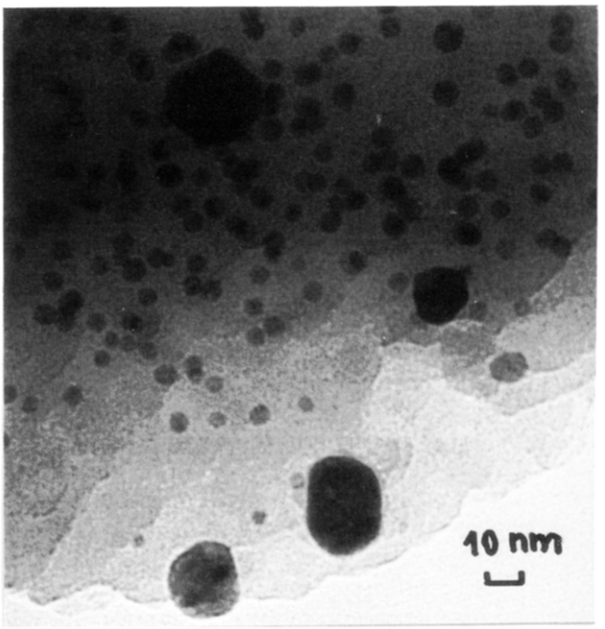

Figure 1. TEM of **2** ($Pd_{0.7}Ni_{0.3}$·$15SiO_2$).

Table 1. Experimental Lattice Parameters and the Corresponding Composition of the Bimetallic Particles from Transmission Electron Microscopy and Electron Diffraction, Calculated by Using the Data Given in Ref 21b

	particle diam (nm)	lattice param (nm)	exp composition
1	4–6	0.387	$Pd_{0.90}Ni_{0.10}$
	14–20	0.387	$Pd_{0.90}Ni_{0.10}$
2	4–6	0.379	$Pd_{0.66}Ni_{0.34}$
	14–20	0.388	$Pd_{0.92}Ni_{0.08}$
3	4–6	0.376	$Pd_{0.55}Ni_{0.45}$
	14–20	0.388	$Pd_{0.92}Ni_{0.08}$
4	4–6	0.366	$Pd_{0.30}Ni_{0.70}$
	14–20	0.382	$Pd_{0.75}Ni_{0.35}$
5	4–6	0.359	$Pd_{0.14}Ni_{0.86}$
	14–20	0.377	$Pd_{0.60}Ni_{0.40}$

TEM analysis of both **3** (Pd:Ni = 1:1, Figure 3) and **4** (Pd:Ni = 3:7, Figure 4) also shows the presence of small (4–6 nm) and large (14–20 nm diameter) metal particles. Lattice parameters obtained from an electron diffraction analysis are given in Table 1.

Thermomagnetic Investigations. The I_{rel}^{exp} curves obtained from the thermomagnetic measurements are shown in Figure 5. Their convex curvature supports the assumption of bulklike properties of the alloy components. The flat decay of the curves at higher temperatures indicates a distribution of the particle stoichiometry (except **5**).

The composition of the particles can independently be deduced from the Curie temperature (T_c) that is determined by extrapolation of the linear parts of the I_{rel}^{exp} curve to the T axis.[5] The experimental composition determined by this method is given in Table 2.

The temperature dependence of the signal intensity is determined by both the alloy composition and the size of the magnetic crystals. It is additionally influenced by the ratio of the different crystalline phases. Assuming the presence of two phases of the composition C_{Pd} and C_{Ni} (the subscript Pd refers to the Pd-rich phase, the subscript Ni to the Ni-rich phase) in the portions a_{Pd} and a_{Ni}, each of them having a particular average

(4) Mörke, W.; Hirschfelder, M.; Gehre, S.; Doerffel, K. *Chemometrics Intelligent Lab. Syst.* **1990**, *8*, 87.
(5) Robbins, C. G.; Claus, H.; Beck, P. A. *J. Appl. Phys.* **1969**, *40*, 2269.
(6) Engels, S.; Lausch, H.; Mehners, H.-W. *React. Kinet. Catal. Lett.* **1991**, *44*, 251.
(7) Lamber, R.; Jaeger, N. I.; Trunscke, A.; Miessner, H. *Catal. Lett.* **1991**, *11*, 1.

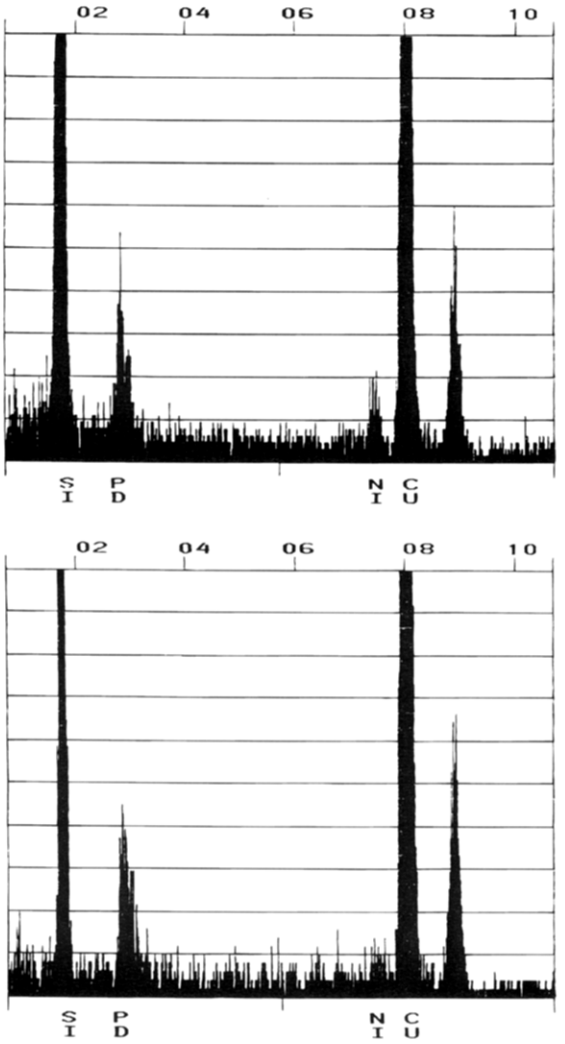

Figure 2. EDX spectrum taken from (a, top) small (4−6 nm) particles a (b, bottom) a large particle of **2**.

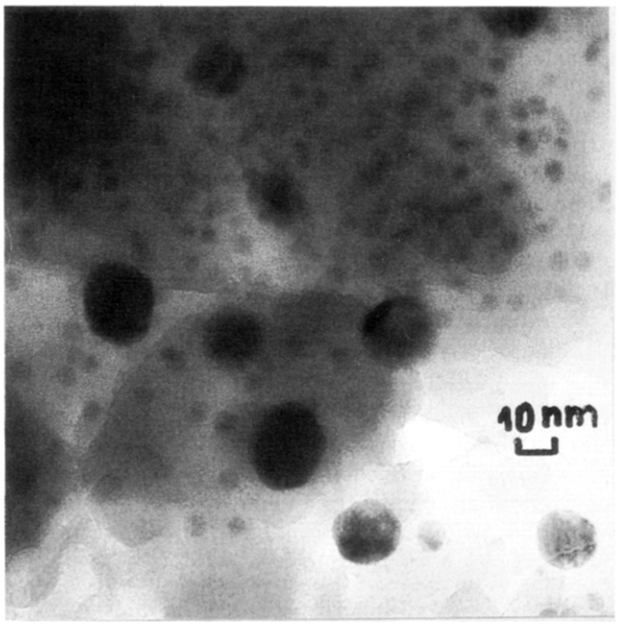

Figure 3. TEM of **3** ($Pd_{0.5}Ni_{0.5}$·15SiO_2).

particle diameter (d_{Pd} and d_{Ni}, i.e., binary particle size distribution of the alloy), and an incomplete reduction of the metals, then six parameters influence the signal intensity.

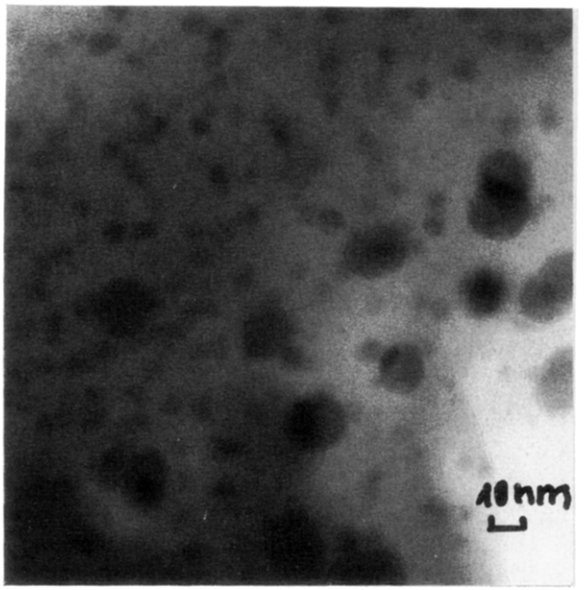

Figure 4. TEM of **4** ($Pd_{0.3}Ni_{0.7}$·15SiO_2).

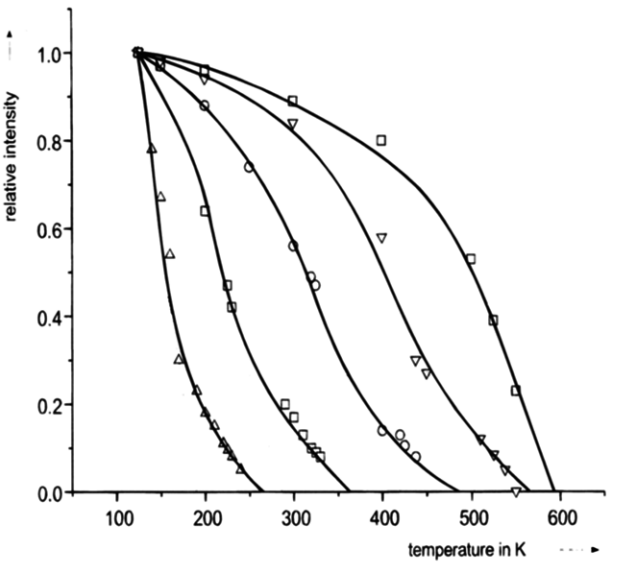

Figure 5. Temperature dependence of the relative integral signal intensity, I_{rel}^{exp}. The full lines correspond to the experimental values. The dotted lines are extrapolations to estimate the Curie temperatures of the Pd-rich alloys. The symbols represent calculated intensity values according to eqs 1 and 2 (**1** (△), **2** (□), **3** (○), **4** (▽), **5** (□)).

Table 2. Experimental Composition of the Alloy Particles from T_c Measurements (C_{Pd} [Atom %], Composition of the Pd-Rich Particles; C_{Ni}, Composition of the Ni-Rich Particles)

	T_{c1}	C_{Pd}	n_1[a]	T_{c2}	C_{Ni}	n_2[a]
1	175	$Pd_{0.89}Ni_{0.11}$	0.22	260	$Pd_{0.82}Ni_{0.18}$	0.37
2	287	$Pd_{0.77}Ni_{0.23}$	0.42	350	$Pd_{0.68}Ni_{0.32}$	0.48
3	420	$Pd_{0.58}Ni_{0.42}$	0.53	490	$Pd_{0.45}Ni_{0.55}$	0.56
4	512	$Pd_{0.41}Ni_{0.59}$	0.58	555	$Pd_{0.32}Ni_{0.68}$	0.59
5	570	$Pd_{0.22}Ni_{0.78}$	0.60			

[a] n is the average number of Bohr's magnetons per atom of the alloy.

C_{Pd} and C_{Ni} can be estimated by T_c measurements (Table 2). The precision of the I_{rel}^{exp} experiments is not sufficient to calculate a_{Pd} and a_{Ni} accurately. Therefore, the particle diameter should be estimated from the I_{rel}^{exp} values in a temperature range where $a_{Ni} = 1$ and $a_{Pd} = 0$, or vice versa. This condition is fulfiled for Ni-rich particles at $T_c^{Pd} < T < T_c^{Ni}$. In the case of Pd-rich

Table 3. Diameters (nanometers) of the Pd-Rich (d_{Pd}) and Ni-Rich (d_{Ni}) Alloy Particles Determined from I_{rel}^{exp} as a Function of T

	C_{Pd}	d_{Pd}	C_{Ni}	d_{Ni}
1	$Pd_{0.89}Ni_{0.11}$	14	$Pd_{0.82}Ni_{0.18}$	4
2	$Pd_{0.77}Ni_{0.23}$	16	$Pd_{0.68}Ni_{0.32}$	4
3	$Pd_{0.58}Ni_{0.42}$	14	$Pd_{0.45}Ni_{0.55}$	8
4	$Pd_{0.41}Ni_{0.59}$	12	$Pd_{0.32}Ni_{0.68}$	4
5	$Pd_{0.22}Ni_{0.78}$	12		

particles we can extrapolate only a very crude upper limit for d_{Pd} from the I_{rel}^{exp} values in the interval 123 K $< T < T_c^{Pd}$ using the approximation $a_{Pd} = 1$, because both Pd-rich and Ni-rich crystallites contribute to the signal intensity. The mean particle sizes d_{Pd} and d_{Ni} were calculated from I_{rel}^{exp} as a function of T according to Griscom's model:[8,9]

$$\frac{I_T^{cal}}{I_{tT}^{cal}} = \frac{M_{S,T}}{M_{S,tT}}\left\{\frac{1-\exp(-2x)}{1-\exp(-(2x+y))}(1-\exp(-y)) + \frac{\exp(-y)}{1-\exp(-y)}\left[\frac{1}{x}(x-y)(1-\exp(-2x)) - (1-\exp(-2(x-y)))\exp(-y)\right]\right\} \quad (1)$$

and are given in Table 3. In eq 1, I_T^{cal} and I_{tT}^{cal} are the calculated signal intensities at the temperature T of the particular measurement and the lowest temperature (123 K), respectively. $M_{S,T}$ and $M_{S,tT}$ are the spontaneous magnetization at these temperatures. x and y are the quotients of the Zeeman energy of a crystallite having a certain composition or of an atom of the alloy, respectively, and the thermal energy ($x = M_{S,T}VB/kT$ or $y = g\mu_B B/kT$, respectively, with V = average volume of a particle, $B = 0.302$ T, k = Boltzmann constant, and $g = g$ factor of an atom of the alloy [$g = 2.22$]). I_T^{cal} and I_{rel}^{exp} are connected by eq 2.

$$I_T^{exp}/I_{tT}^{exp} = I_{rel}^{exp} = I_T^{cal}/I_{tT}^{cal} \quad (2)$$

Simulation of the FMR Powder Spectra. The chemical composition of the alloy particles can be further verified by simulation of the FMR powder spectra, if the dominant kind of anisotropy and its dependence on the composition is known. The magnetic dipolar interaction between the particles can be neglected, because they are diamagnetically diluted, spherical crystallites (Figures 1, 3, and 4). Thus every crystallite contributes to the resonance independent of the others. In this case the equilibrium position of the magnetization vector is determined by the magnetocrystalline anisotropy, dominant in these particles. The FMR powder spectrum is then determined only by the distribution function ($\Omega(B)$) of the resonance ($B_r(\theta_B,\Phi_B)$) of the individual crystallites with different orientation relative to the external magnetic field.[10] θ_B and Φ_B are the spherical angles between the direction of B and the main axes of the crystallites. Schlömann showed that in the case of a large crystal anisotropy the equilibrium position of the magnetization vector does no longer align with the direction of B but is distorted toward the direction of the easier magnetization.[10] $B_r(\theta_B,\Phi_B)$ is then calculated at the stationary points, i.e., the [100], [110], and [100] direction, according to the Smith–Suhl method:[11,12]

$$B[100] = B_0(1 + k')$$

$$B[110] = B_0(1 + {}^9/_{16}k'^2)^{1/2} - {}^1/_4k'$$

$$B[111] = B_0(1 - {}^2/_3k') \quad (3)$$

with $B_0 = h\nu/g\mu_B$ and

$$k' = -2K_{1,T}/M_{S,T}\cdot B_0 \quad (4)$$

where $K_{1,T}$ is the first order magnetocrystalline constant, and $M_{S,T}$ is the spontaneous magnetization.[10] The distribution function $\Omega(B)$ is approximated by the sum of its singular part $u_s(x)$ and a suitable trial function $u_t(x)$ with five free parameters, where $u_s(x) = -\alpha \ln|x - x_0|$, and $u_t(x)$ is a polynominal or more complicated logarithmic function being parametrized by fitting exactly the heights and slopes of $\Omega(B)$ at the finite steps at the ends of the interval.[10] α, x, and x_0 are k'-dependent variables as outlined in ref 10. The results of the two trial functions agree closely if the anisotropy k' is small ($k' \leq 0.5$). The superposition of the spectra corresponding to different values $K_{1,T}$ was done in the following way: the distribution functions $\Omega(B)$ for three different $K_{1,T}$ values were weighted, added, and then convoluted with the first derivative of a Lorentz line form function of the half-width ΔB.

To interpret k', one has to know the dependence of $K_{1,T}$ and $M_{S,T}$ on the chemical composition of the alloy, and the dependence of $K_{1,T}$ on the particle size. An influence of the particle size on the experimentally estimated anisotropy energy is expected, if the particles are superparamagnetic.[13] Superparamagnetism or ferromagnetism is related to the time scale of the FMR experiment, the measuring time t_m in our experiments being 1.08×10^{-10} s. The particles behave superparamagnetically, if the relaxation time τ of the microcrystals is smaller than t_m. τ was calculated by means of the high-energy approximation ($K_{1,123}V/kT \gg 1$).[14] We found that the Ni-rich particles of the samples **2**–**5** with $d \approx 5$ nm are ferromagnetic at 123 K.

$K_{1,T}$ as a function of the Pd content in Ni/Pd alloys and the temperature is given in ref 15. $M_{S,T}$ was calculated from the temperature dependence of the spontaneous magnetization, starting from $M_{S,0}$ by the Brillouin function.[16] $M_{S,0}$ is obtained from the average number of Bohr's magnetons per atom of the alloy (n) (Table 2).[17] $K_{1,123}$ has a negative sign at higher Ni contents, which becomes positive at about 50 atom % Pd and reaches zero at about 95 atom % Pd.[15] The spectral simulations were started with a parameter set deduced from TEM results (Table 1). The distribution

(8) Griscom, D. L. *IEEE Trans. Magn.* **1981**, *17*, 2748.
(9) Châtelain, A.; Buffat, P.; Stadelman, P.; Weeks, R. A. *J. Non-Cryst. Solids* **1985**, *71*, 335.
(10) Schlömann, E. *J. Phys. Chem. Solids* **1958**, *6*, 257.
(11) Smit, J.; Beljers, H. G. *Philips Res. Rep.* **1955**, *10*, 119.
(12) Suhl, D. *Phys. Rev.* **1955**, *97*, 555.
(13) De Biasi, R. S.; Devezas, T. C. *J. Appl. Phys.* **1978**, *49*, 2466.
(14) Morup, S.; Dumesic, J. A.; Topsoe, H. *Application of Mössbauer Spectroscopy*; Cohen, R. L., Ed.; Academic Press, New York, 1980; Vol. II, p 15.
(15) *Landolt-Börnstein*, Neue Serie Bd. 19a; Springer: Berlin, 1986; p 624.
(16) Kneller, E. *Ferromagnetismus*; Springer: Berlin, 1962; p 33.
(17) Kneller, E. *Ferromagnetismus*; Springer: Berlin, 1962; p 241.
(18) Griscom, D. L.; Friebele, E. J.; Shinn, D. B. *J. Appl. Phys.* **1979**, *59*, 2402.

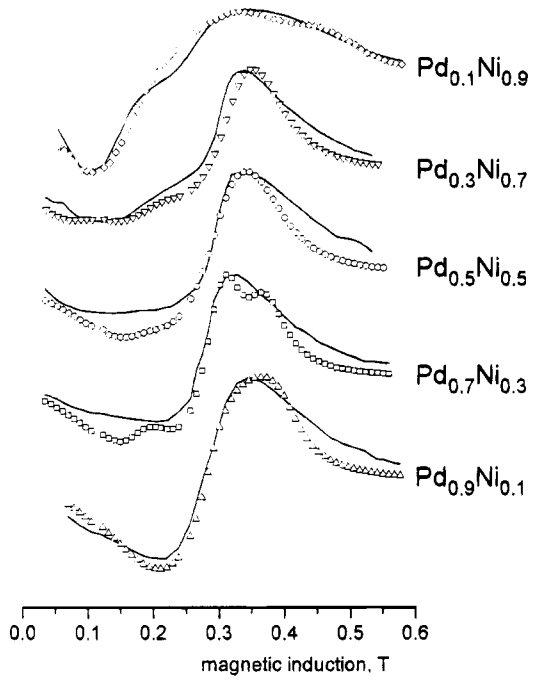

Figure 6. Experimental and calculated FMR powder spectra of **1**–**5** recorded at 123 K. The full lines correspond to the experimental values, the symbols to calculated values. The parameters of the spectra calculation are given in Table 5.

function of $\Omega(B)$ was approximated for $k' < 0.5$ by a polynomial and for $k' > 0.5$ by a logarithmic function to simulate the experimental spectra.[10]

No suitable fit between the calculated and experimental spectra was obtained with a set of parameters ($K_{1,123}/M_{S,T}$, B_0, and ΔB) corresponding to the model, because the experimental resonance field was shifted to lower values compared with the calculated spectra. The fit was only improved by lowering $B_{r,123}$ significantly relative to B_0. By doing so, k' in **5** became larger than 0.8. The failure of the model with regard to B_0 could be due to the fact that the interpolation procedure for the calculation of the distribution function[10] was not applied in this case. (We thank a referee for drawing our attention to that.) However, the differences between $B_{r,123}$ and B_0 were also found in the samples with $k' < 0.8$. We therefore believe that the main reason for this is the neglection of additional magnetoelastic interactions in the model (vide infra). Such interactions shift the resonance field isotropically and may change the appearance of the FMR spectra.[19,20]

If the independent grain approach with large anisotropy covers the major physical influences except an additional isotropic shift of the signal, it is not justified to conceal this deficiency by an increase in the number of parameters, although there is a better fit for FMR powder spectra when a distribution function is used for $K_{1,123}$.[18] Therefore, the number of alloy compositions was deliberately restricted to three. This also allows a better comparison with the electron diffraction results.

The experimental and calculated spectra of the compounds **1**–**5** are compared in Figure 6. Table 4 gives the alloy composition as determined by the spectral simulations. Table 5 contains the parameters of the calculated FMR powder spectra.

Table 4. Composition of the Alloy Particles from the Spectral Simulations

	composition 1	composition 2	composition 3
1	Pd content ≥ 90 atom %		
2	$Pd_{0.7}Ni_{0.3}$	$Pd_{0.7}Ni_{0.3}$	$Pd_{0.9}Ni_{0.1}$
3	$Pd_{0.55}Ni_{0.45}$	$Pd_{0.75}Ni_{0.25}$	$Pd_{0.9}Ni_{0.1}$
4	$Pd_{0.3}Ni_{0.7}$	$Pd_{0.8}Ni_{0.2}$	$Pd_{0.9}Ni_{0.1}$
5	$Pd_{0.1}Ni_{0.9}$[a]		

[a] This is an average value, because the $K_{1,123}$ values in the range between $Ni_{1.0}$ and $Ni_{0.8}Pd_{0.2}$ cannot be distinguished from each other.[18]

Table 5. Parameters of Spectral Simulations. Numbers in Brackets Are the Weighing Factors of the Particular Composition for the Spectral Simulations

	$K_{1,123}/M_{S,123}$ (mT)	$B_{r,123}$ (mT)	B_{pp}[a] (mT)	σ[b]
1	1	262.5	60 (1)	0.06
	1	250.0	60 (1)	
	1	285.0	60 (1)	
2	9.4	300.0	25 (1)	
	94	252.0	25 (1)	0.07
	94	200.0	25 (1)	
3	10	290.0	35 (1)	
	80	240.0	35 (1)	0.12
	110	210.0	35 (1)	
4	−95	220.0	30 (1)	
	60	280.0	30 (1)	0.07
	10	300.0	30 (1)	
5	−112	220.0	20 (1)	
	−112	270.0	20 (1)	0.03
	−112	300.0	20 (0.5)	

[a] Peak-to-width of the derivatives of the convolution function. [b] Approximation error = $((I_{rel}^{exp} - I_{rel}^{cal})^2/(\text{number of data points} - 1))^{1/2}$, which describes the goodness of the fit.

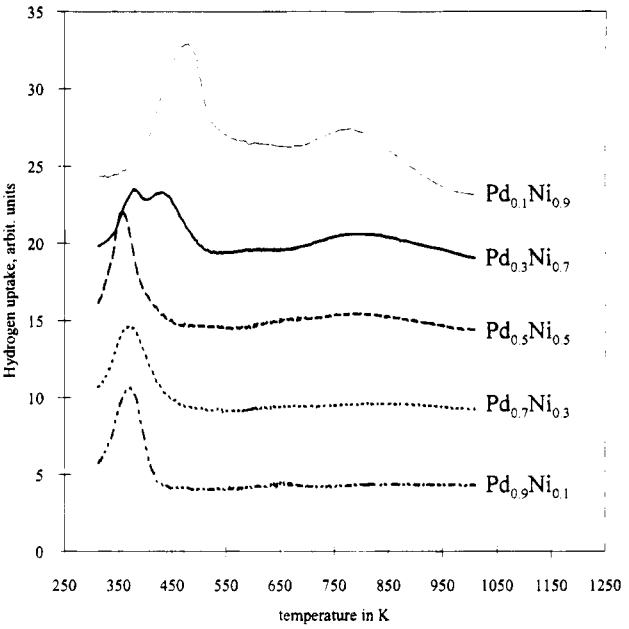

Figure 7. TPR curves of **1**–**5**.

Temperature-Programmed Reduction. The TPR results are shown in Figure 7. The maxima of the H_2 consumption at about 380 K are caused by the reduction of Pd-rich mixed-metal oxide crystallites. The range around 750 K corresponds to the reduction of mixed metal oxide particles Pd_xNi_yO and/or NiO. Reduction temperatures above 750 K are due to the presence of nickel silicates. The high-temperature peak is most pronounced for the two samples with the lowest Pd content.

(19) Suran, G.; Stankoff, A.; Hoffmann, F. *Phys. Rev. B.* **1973**, *8*, 1109.
(20) Kotyukov, Yu. N.; Abrosov, V. *Sov. Phys. J.* **1972**, *15*, 1.

Discussion

Metal Particle Composition and Size. Palladium and nickel are miscible for any atomic ratio and form fcc solid solutions with the lattice constants in the range 0.3523 (100% Ni) to 0.3890 nm (100% Pd).[21] EDX analysis of the small and large alloy particles (Figure 2) shows some differences in their composition. A reliable quantification of the EDX spectra could not be achieved, because the small number of counts accumulated under each peak gave rise to a large statistical error. Nevertheless, an estimation of the atomic concentration of Pd in the small and large alloy particles is possible from the changes of the lattice parameters. The results of this estimation are given in Table 1.

Inspection of Table 1 shows that the composition of small particles (4–6 nm) is very close to the nominal composition of the Pd–Ni specimen. The large particles (14–20 nm) have a much higher palladium content. Therefore, the EDX and TEM measurements indicate a bimodal distribution in both composition and size.

These results have to be compared with the particle compositions determined from the magnetic measurements. The relation between the alloy composition and the primary ($M_{S,T}$) and secondary ($K_{1,T}$) magnetic properties, used for the thermomagnetic measurements and the spectral simulations, results in a larger weight for the Ni-rich components. Therefore, alloy particles with the biggest k' (Ni-rich particles) dominate the spectra and the I_{rel}^{exp} curves, and the Pd-rich species only are difficult to identify. In addition, T_c of the Pd-rich components is determined in a temperature range in which both Pd-rich and Ni-rich crystallites contribute to I_{rel}^{exp}. T_c of the Pd-rich species only can be determined, if their contribution to the total magnetization of the sample is big enough to result in a distinct drop in the I^{exp}_{rel}–T curve at T_c.

The results of the electron microscopic investigations of **1**–**3** suggested that the portion of the Pd-rich particles (with a nearly constant Pd content of 90–92%) becomes smaller with increasing overall Ni content. This results in a distinct shift of T_c of the Pd-rich particles to higher temperatures. As a consequence, the crystallites seem to contain a higher Ni content compared with the ED results (see samples **1** and **2** in Tables 1 and 2). In extreme cases the Pd-rich particles cannot be found, because their contribution to the total magnetization is too low (see samples **3** and **4** in Tables 1 and 2).

Pd-rich species were found by the TEM investigations (Table 1). The notion of both a bimodal particle size distribution and bimodal composition distribution that results from the TEM measurements must be corrected by the TPR measurements and the spectral simulations. Since the Ni-rich particles have approximately the nominal composition and the other particles are richer in Pd, there has to be additional, probably unreduced nickel in the bulk of the material.

Determination of the chemical composition by fitting $K_{1,T}$ to the experimental FMR spectrum is ambiguous for Pd contents larger than 50 atom % (one $K_{1,123}$ value corresponds to two c_{Pd} values). The species with 45% and 41% Pd in **3**–**5** cannot be reproduced by spectral simulations alone, because the weight of the $K_{1,123}$ values in these samples is dominated by the big $K_{1,123}$ values.

Keeping these effects in mind, there is a sufficiently good correlation between the TEM and magnetic measurements.

From studies on reduction of the metals and formation of alloy particles in zeolite cages containing either Pd^{2+} and Ni^{2+} ions, or Pd^{2+} ions and small NiO clusters it is known that Pd enhances the reducibility of Ni. Upon reduction with H_2 either Pd atoms migrate to NiO clusters, or Ni ions to Pd particles, or PdNi dimers are formed.[22] We do not know the composition of the metal oxide particles before reduction. However, their size is in the lower nanometer range. We therefore are presently unable to say whether the observed composition distribution stems from the oxidation step or the reduction step or both. After oxidation there can be three types of particles: pure NiO, pure PdO or mixed Pd_xNi_yO. Additionally there may be Ni^{2+} or (less likely) Pd^{2+} ions bonded to $Si-O^-$ groups of the gel network. PdO and Pd_xNi_yO is easier reduced than NiO particles or Ni^{2+}. Therefore, Pd and Pd_xNi_y crystallites are probably formed at relatively low temperatures (see Figure 7). Figure 7 also shows that the peaks at about 370–470 K characteristic for the reduction of the Pd-rich particles are shifted to higher reduction temperatures with increasing Ni content. This indicates that the uptake of H_2 becomes more difficult and that the Pd content of the Pd-rich particles is lowered. There is additional H_2 uptake at about 773 K in samples **3**–**5**. In this range, Ni-rich Pd_xNi_yO species and/or NiO are reduced.

The concentration of Pd in the metal particles in the early stages of the reduction depletes Pd in the bulk of the material. Possibly only those Ni ions (or NiO particles) are reduced which can be reached by the migrating Pd atoms or which can migrate to Pd or Pd_xNi_y clusters. For the complete reduction of other Ni^{2+}-containing species (Ni–silicate or NiO) the employed temperature of 773 K may not be sufficient.

Another possible explanation for the presence of Ni^{2+} in the reduced materials is reoxidation of Ni at high temperatures by protons created during reduction.[22] In NiPd-containing zeolithes, up to 30% Ni were reoxidized at 773 K, leading to dealloying by selective leaching of Ni from the bimetallic particles.[22]

Metal–Matrix Interaction. The magnetic anisotropy dominates the equilibrium position of the magnetisation vector and therefore the FMR powder spectra. The magnetic field B_{eff}, determined from zero of the derivative curve, should correspond for this kind of anisotropy to the anisotropy field ($2K_{1,T}/M_{S,T}$, eq 5).[23]

$$B_{eff} = B_0(g = 2.22) + K_{1,T}/M_{S,T}/2 \qquad (5)$$

According to the magnitude of the anisotropy field recorded in Table 5, B_{eff} should be between 0.24 and 0.3 T for $K_{1,123} < 0$ (samples **4** and **5**). In the case of $K_{1,123} > 0$ (samples **1**–**3**) B_{eff} should be >0.32 T. However, to reach a good fit between experimental and calculated

(21) (a) Hansen, M. *Constitution of Binary Alloys*, 2nd ed.; McGraw-Hill: New York, 1958. (b) Bidwell, L. R.; Speiser, R. *Acta Crystallogr.* **1964**, *17*, 1473.

(22) Feeley, J. S.; Sachtler, W. M. H. *Zeolites* **1990**, *10*, 739; *J. Catal.* **1991**, *131*, 573.

(23) Sharma, V. K.; Baiker, A. *J. Chem. Phys.* **1981**, *75*, 5596.

spectra, one has to calculate the spectra with a B value ($B_{r,123}$) smaller than B_0 and smaller than B_{eff}.

We suppose that the reason for this distinct shift of the resonance field relative to the field caused by crystal anisotropy is a mechanical influence on the metal particles. Such influences are not taken into account by the applied model. A mechanical influence can be due to alloying,[24] surface tension,[25] and/or differences in the thermal expansion coefficient between the metal particles and the matrix.[26] Compressive ($\delta < 0$) or tensile stress ($\delta > 0$) can act via the magnetostrictive properties of the alloy crystallites as an additional field (B_r; λ_s, the magnetostriction constant of Ni and its alloys with Pd is negative[15]):

$$B_r = 3\lambda_s\sigma/M_{s,123} \quad (6)$$

The surface tension of small crystallites results in $\sigma_\tau < 0$.[25] The different thermal expansion coefficients α_M (metal) and α_S (matrix) result in a compressive strain (σ_T) on the crystallites:[27]

$$\sigma_T = (\alpha_M - \alpha_S)E\Delta T \quad (7)$$

E being the Young's modulus of the metal.

Both effects would shift B_{eff} to higher values, opposite to the experimental and theoretical B values. There is obviously tension on the metal particles that in our opinion is caused by the present unreduced Ni^{2+} (Figure 7), which probably anchors the alloy particles to the matrix. The positively charged metal ions withdraw electron density from the metal atoms in the particles. This results in incompletely screened nickel atoms, which try to increase their equilibrium distance and cause tensile stress within the particles. This stress is increased by partial replacement of the Ni atoms in the crystal lattice by the larger Pd atoms, favoring larger equilibrium distances. As long as unreduced Ni ions are present, σ is larger than zero for the Ni/Pd alloy particles. Since the magnitude of λ_s depends on the Pd content,[15] the magnitude of σ on the number of anchoring atoms per particles and on the Pd/Ni atoms per particle, we expect a distribution of B_r values (see Table 5). This distribution is superimposed by a distribution function of $K_{1,123}$ values. Both together are roughly described by the weighing factor in Table 5. Thus, three factors influence the difference between B_0 and $B_{r,123}$, namely alloying, the presence of unreduced Ni ions in the crystals, and the change of λ_s with the Pd content. From the difference between B_{eff} and $B_{r,123}$, we estimate the order of σ from 10^6 to about 6×10^8 Pa. Values of σ in this order of magnitude are typical for poly- and monocrystalline thin Ni films.[28] The conclusion that there is considerable tension in the alloy particles is supported by the magnitude of the anisotopic field in the Ni-rich crystallites. Crystallites having a diameter of about 5 nm (Table 1) should show a reduced anisotropy field at 123 K owing to fluctuations of the magnetization vector around the easy direction.[29] We suppose that the magnetocrystalline anisotropy is amplified by mechanical stress, because we cannot detect such a behavior. This possibility was already pointed out by Suran et al.[19] and Kotyukov et al.[20]

Conclusions

We showed that small alloy particles can be prepared by the same method which led to highly dispersed monometallic particles in SiO_2. In a series of materials having the nominal composition Pd_xNi_{1-x}·$15SiO_2$ a bimodal particle size distribution with particles around 4 and 15 nm was found. The size distribution is similar to that of dispersed Ni particles prepared by the same method.

According to the magnetic measurements the composition distribution is rather complicated. The composition of the particles with the highest Ni content approximately corresponds to the nominal composition, independent of x. By interpretation of the FMR spectra, other particle compositions are found with lower Ni contents. To balance the starting composition, additional Ni species must be present which cannot be seen by electron diffraction or EPR spectroscopy. We conclude that these species must be nickel silicate species. Incomplete reduction of the less noble metal is not unusual when bimetallic metal particles on solid supports are prepared (e.g., refs 22 and 30).

Mixing of the two metal components during the initial sol–gel step must be very homogeneous, because no monometallic particles were found. The results therefore are a promising onset for the development of highly dispersed alloy particles by the sol–gel method. Future work has to be directed toward the optimization of the parameters influencing the particle composition distribution.

Acknowledgment. The work was supported by the Fonds der Chemischen Ind. and the Deutsche Forschungsgemeinschaft. The authors are also grateful to Dr. H. Lausch and Mr. Koschel for their help with the TPR measurements, and to Mrs. S. Stevenz for her assistance with the FMR measurements.

(24) Takahashi, H.; Tsunashima, S.; Fukatsu, S.; Uchiyama, S. *J. Magn. Magn. Mater.* **1990**, *93*, 469.
(25) Janssen, M. M. P. *J. Appl. Phys.* **1970**, *41*, 384.
(26) Chapra, K. L. *Thin Film Phenomena*; McGraw-Hill: New York, 1979; p 271.
(27) Bonneviot, L.; Che, M.; Olivier, D.; Martin, G. A.; Freund, E. *J. Phys. Chem.* **1986**, *90*, 2112.
(28) Shih, C. Y.; Bauer, C. J.; Artmann, J. O. *J. Appl. Phys.* **1988**, *64*, 5428.
(29) Morup, S. *J. Magn. Mater.* **1983**, *37*, 39.
(30) Guerrero-Ruiz, A.; Sepulveda-Escribano, A.; Rodriguez-Ramos, I. *Appl. Catal., Part A* **1992**, *81*, 81.